

Computer Methods in Biomechanics and Biomedical Engineering: Imaging & Visualization

ISSN: (Print) (Online) Journal homepage: <https://www.tandfonline.com/loi/tciv20>

Patient-specific CFD simulation of aerodynamics for nasal pathology: a combined computational and experimental study

Nazym S. Sagandykova , Ildar R. Fakhraiyev , Sreekar Reddy Sajjala , Saule A. Taukeleva , Dinara E. Shemetova , Timur M. Saliev , Shynar B. Tanabayeva & Yong Zhao

To cite this article: Nazym S. Sagandykova , Ildar R. Fakhraiyev , Sreekar Reddy Sajjala , Saule A. Taukeleva , Dinara E. Shemetova , Timur M. Saliev , Shynar B. Tanabayeva & Yong Zhao (2021): Patient-specific CFD simulation of aerodynamics for nasal pathology: a combined computational and experimental study, Computer Methods in Biomechanics and Biomedical Engineering: Imaging & Visualization, DOI: [10.1080/21681163.2020.1858968](https://doi.org/10.1080/21681163.2020.1858968)

To link to this article: <https://doi.org/10.1080/21681163.2020.1858968>



Published online: 15 Feb 2021.



Submit your article to this journal



Article views: 33



View related articles



View Crossmark data



Patient-specific CFD simulation of aerodynamics for nasal pathology: a combined computational and experimental study

Nazym S. Sagandykova ^a, Ildar R. Fakhraiyev ^b, Sreekar Reddy Sajjala ^c, Saule A. Taukeleva ^a, Dinara E. Shemetova ^a, Timur M. Saliev ^b, Shynar B. Tanabayeva ^b and Yong Zhao ^d

^aDepartment of Otorhinolaryngology, Kazakh Medical University of Continuing Education, Almaty, Republic of Kazakhstan; ^bExperimental Medicine Laboratory, S.D. Asfendiyarov Kazakh National Medical University, Almaty, Republic of Kazakhstan; ^cMechanical Engineering, SoET, BML Munjal University, Gurgaon, India; ^dDepartment of Mechanical Aerospace Engineering, School of Engineering, Nazarbayev University, Nur-Sultan, Republic of Kazakhstan

ABSTRACT

The aim of this study was to develop and verify a personalised approach for simulating the aerodynamic flow patterns using patient-specific data of a severe form of nasal obstruction during inspiration. The reconstruction of the 3D geometry of the nasal cavity based on the computer images of a patient diagnosed with the unilateral nasal valve collapse and S-shaped septum deviation was used to perform the Computational Fluid Dynamics (CFD) simulation of airflow. A comparative study of the airflow with standard data (SD) and personal input data (PD) of mass flow rate was carried out. In both cases, the air streamlines went straight along the lower and middle nasal passages on the non-deviated septum side. The peak velocity increased in two cavities, mostly on the septum deviation side, while the peak pressure inversely dropped. With personal data, the peak velocity and pressure values varied greatly in different parts of the nasal cavity, depending on the particular local anatomy. In a patient with unilateral nasal valve collapse and S-shaped septum deviation, the use of personal data does not have an impact on the streamline's direction, longitudinal velocity, and pressure distributions but it significantly changed the local velocity and pressure in the nasal cavity.

ARTICLE HISTORY

Received 14 August 2020
Accepted 30 November 2020

KEYWORDS

CFD simulation; nasal vestibule; septum deviation; mass flow rate; velocity

1. Introduction

Despite the recent progress, the local nasal processes such as heat-moisture exchange and the interaction of airflow with the surface of the nasal mucosa have not been fully studied and reported yet (Elad et al. 2008).

In fact, the anatomy of the nasal cavity and the mechanisms of physiological processes are highly complex due to the presence of many small passages and connections within the paranasal sinuses. Moreover, nasal turbulent aerodynamics, local heat transfer and fluid phase change are still poorly understood. In this regard, common assessment methods can provide limited information and have a low correlation with subjective feelings of patients (Sipilä et al. 1995; Hirschberg and Rezek 1998; Hsu et al. 2017; Desvant et al. 2018).

During recent decades, the Computational Fluid Dynamics (CFD) simulation technique has been increasingly used for the detailed study of nasal aerodynamics. A range of studies have been focused on obtaining the information about turbulent airflow, heat transfer and fluid phase change in the nasal cavity not only in a healthy person but also in a patient with different pathologies (Zhao et al. 2004; Wen et al. 2008; Liu et al. 2012).

To perform the simulation, the boundary conditions are prescribed for the wall, inlet, and outlet of the airway, which includes mass flow rate, air pressure, and nasal cavity wall rigidity. Standard population-averaged input data have been utilised to improve simulation results (Riazuddin et al. 2011; Chen et al. 2009).

For example, a volumetric flow rate of 15 to 20 l/min has been used (as a standard rate) that is typical for human breath at rest (Enberg and Ownby 1991). However, the flow rate varies greatly depending on the respiration phase, gender, and selected time of measuring (Cho et al. 1997). In fact, the airflow rate can reach up to 150 l/min in case of nasal obstruction (Hooper 2001). Thus, more than 80% of patients with a complex form of septum deviation and valve pathology have a much higher flow rate than healthy subjects (Huygen et al. 1992). The PIV (Particle Imaging Velocimetry) study by (Doorly et al. 2008a; 2008b), where simulations were carried out at different speeds, was dedicated to the validation of laminar flow assumption at a rate of 15–20 l/min.

There is a range of attempts to perform the nasal airflow simulations followed by the comparison of the results on a variable value of input data (Riazuddin et al. 2011; Xiong et al. 2008; Chen et al. 2009; Xi et al. 2016). In fact, the increase of mass flow rate induced the appearance of new vortex zones, significant changes in streamlines and pressure in various areas of healthy and pathological nasal cavities. Very often the magnitude of the input flow rate was determined based on the choice of the flow type: laminar flow (≤ 20 l/min) and turbulent (≥ 20 l/min) (Chen et al. 2009). However, the anatomical variation of the nasal cavity has not been taken into account regarding the choice of flow rate and has not been reported yet. Some researchers have criticised the CFD simulation procedure due

to the lack of a patient-specific approach (Bavo et al. 2016; Cherobin et al. 2018).

Therefore, only a personalised approach based on the anatomical specificity of the nasal cavity, including the nasal valve pathology and the nasopharynx size, might significantly improve the results of CFD modelling (Taylor et al. 2010; Quadrio et al. 2014; Bavo et al. 2016).

Taking into account the above-mentioned issues, this study aimed at the assessment of a personalised approach for the CFD modelling in the patients with a complex form of nasal obstruction.

2. Materials and methods

2.1. Ethical issues

The study was carried out using CT images of the nasal cavity and the data from active anterior rhinomanometry taken from a patient at the ENT department at a specialised clinic (City Hospital No. 5) in Almaty, Kazakhstan. Informed consent was obtained prior to the study. The study was approved locally by the High Ethical commission of KazMUCE, Almaty, Kazakhstan (protocol No. 1, dated 15 January 2019).

2.2. The patient characteristics

The patient, 44 years old, had the following diagnosis: bilateral pathology of the nasal cavity, S-shaped nasal septum deviation (anterio-posterior direction) (Figure 1(a)) and the right nasal valve collapse (Figure 1(b)). The nasal cavity had a prominent posterior part on the left side adjoining to the inferior nasal turbinate (Figure 1(c)). The anatomical structure's pathology in the nasal cavity caused nasal obstruction syndrome (for this patient): nasal congestion, trouble breathing through nose and sleeping trouble. This feature makes it possible to compare two different nasal pathologies in one patient. Moreover, it allowed to investigate the combined effect of these pathologies (with different input data).

2.3. Data retrieval

To measure the total amount of air passing through the airway per unit time (volumetric flow rate) and the resistance, the patient was tested by active anterior rhinomanometry

(Otopront RHINO-SYS, Germany). The data were obtained in accordance with the recommendations of the Standardisation Committee (Clement and Gordts 2005). 20 minutes before the study, 0.05% oxymetazoline was topically administrated (in the rest room) by 2 sprays (0.1 ml) into each nostril, repeated after 5 minutes. The rhinomanometry was carried out in a sitting state, after 15 minutes of rest. The flow rate was measured using a breathing mask with a special highly sensitive sensor. The obtained data were recorded as a curve on an electronic device separately for each half of the nose during inhalation. CT images were obtained by using a SOMATOM computer tomography (Emotion 16, Siemens, Germany). The images were taken in three projections: axial, coronary, and sagittal with a slicing step of 0.5 mm (Quadrio et al. 2014).

2.4. CFD Modelling

2.4.1. Creating 3D geometry

Specialists in softwares MIMICS MEDICAL 22.0 (Leuven, Belgium) and 3-matic Medical 14.0 (Leuven, Belguim 2019), who previously participated in a similar biomedical study, took part in the creation of 3D geometry. The 3D Geometry was constructed with the participation of a clinical rhinologist for the best accuracy of the anatomical zones chosen.

241 computer slices of the DICOMDIR format were imported into Mimics Medical version 22.0 (Leuven, Belgium). All procedures were performed according to the proposed guidelines provided by the software developer. The threshold level was set between -1024 and 317 Hounsfield units to separate air from other elements, according to the recommendations by published works (Cherobin et al. 2018). Since the experiment estimated airflow only in the nasal cavity, it was necessary to separate the paranasal sinuses. Manual adjustments were made to remove thin bones in the ethmoid region, as well as to separate the frontal and maxillary sinuses.

The resulting files (STL) were imported into Materialise 3-matic® Medical version 14.0 (Leuven, Belguim 2019) to fix and remesh the surfaces. For the meshing parameters 0.6 mm as the maximum length of the triangle edge was established. To use the current object for simulation the following changes were made:

Obstructed areas (Figure 2) created as artefacts during data collection and geometric modelling in the 3D model of the nasal cavity were excluded.

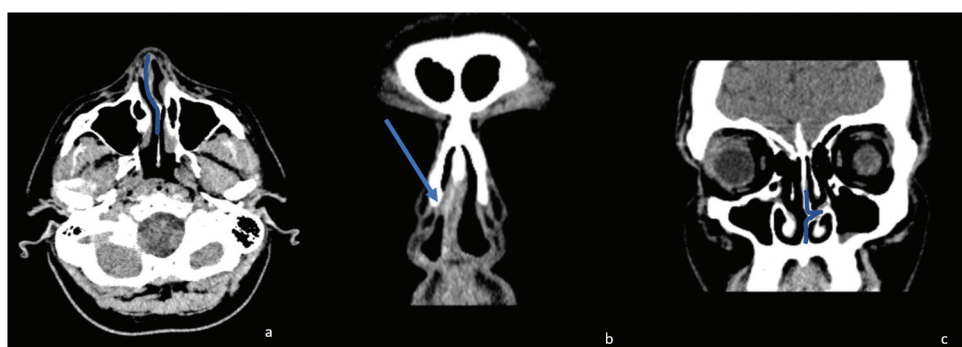


Figure 1. Patient (44 years old), diagnosis: bilateral pathology of the nasal cavity. (a) S-shaped septum deviation (axial view), (b) right-sided nasal valve collapse (coronal view), (c) the posterior part of nasal septum deviation (coronal view).

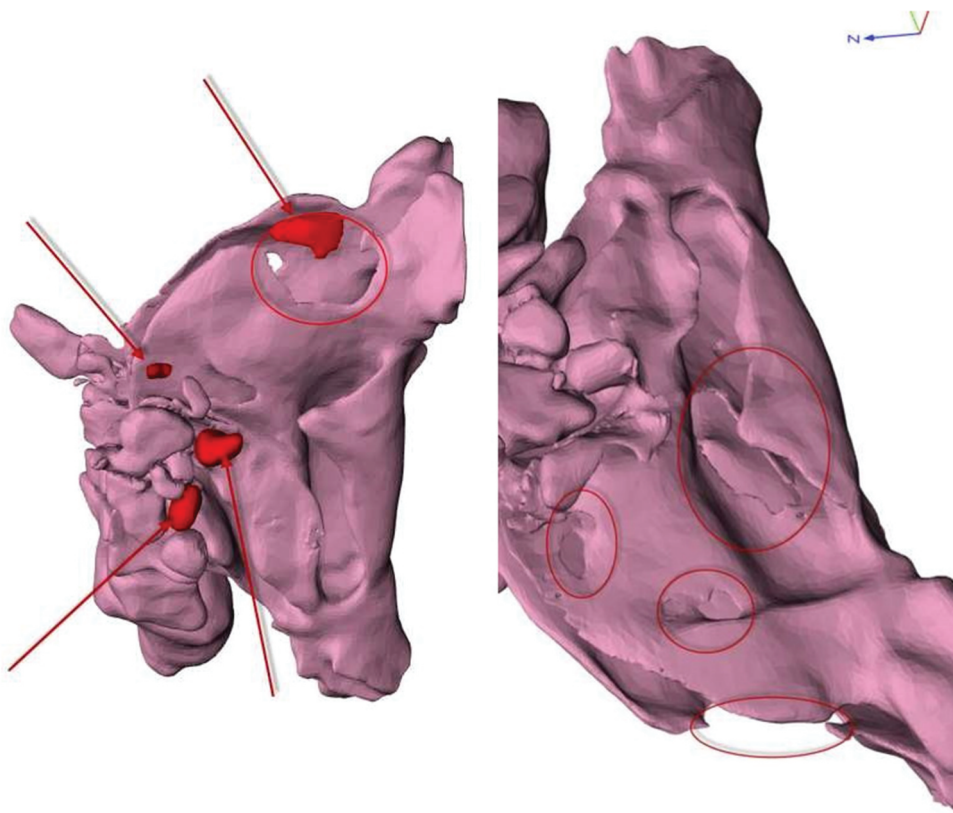


Figure 2. Obstructed areas on the 3D model of the nasal cavity.

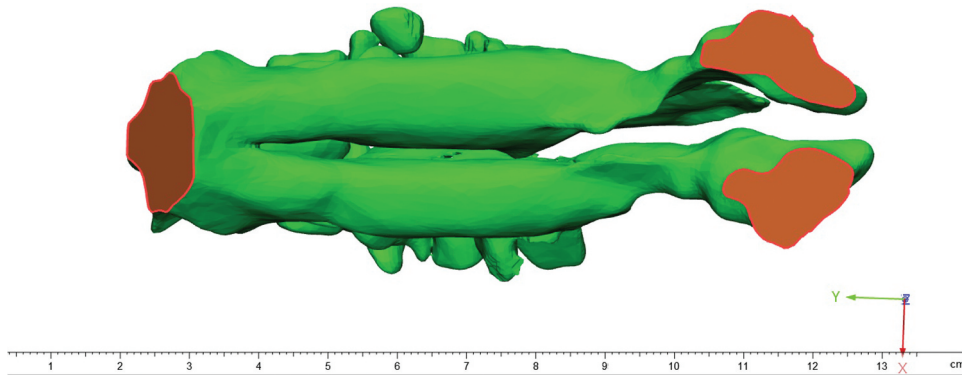


Figure 3. Inlet (orange) and outlet surfaces (red coloured).

Separate surfaces for input/output (Figure 3) were formed, where the lower part of the model had two surfaces defining the inlets of the nostrils.

Thin walls with a pitch of less than 0.1 mm were expanded to 0.3 mm to avoid geometry errors (Figure 4).

2.4.2. Creating a solid model and computational grids

The creation of a solid model, grids, the introduction of input data and the simulation were carried out. The resulting 3D model was exported to ANSYS Fluent

19.2 (ANSYS Inc., Canonsburg, PA), where it was converted to a 3D solid model, which was then discretized with a tetrahedral grid (Tet10). Inflation was implemented automatically to further divide the mesh into fine multiple layers at proximity zones near the walls, and at the Dirichlet boundary

condition regimes. The mesh density was not identical, with narrower areas having higher mesh density. Therefore, the number of elements in wall proximity regions was comparable that of the inner core region.

To discretise the model, a very fine grid of 4,894,368 elements was created with an element asymmetry of less than <0.3 and an element quality of 0.87.

2.4.3. Boundary conditions

The simulation of the stationary state with standard data (SD) was obtained by applying a gauge pressure of 0 Pa at the nostrils as the inlet conditions, and the outlet a uniform flow rate of 15 l/min as boundary condition. The rest of the geometry was defined as a no-slip wall condition (Chen et al. 2009).

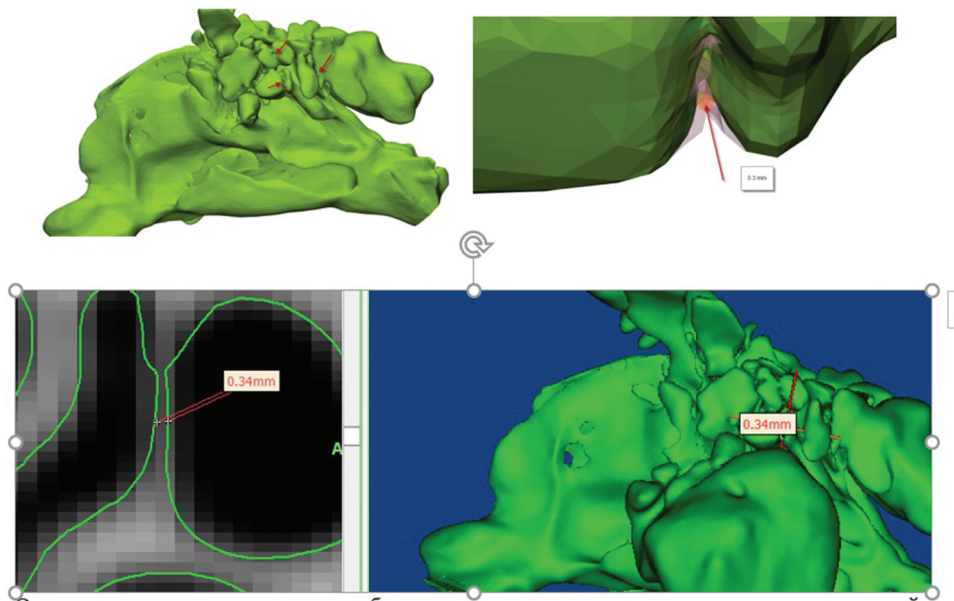


Figure 4. The expanded walls of the nasal cavity geometry.

A simulation of the stationary state with personal data (PD) flow data was performed with a flow rate at the outlet set to 57 + 16 l/min at the outlet, corresponding to the sum of the left and right nostril flow rates. The reason to prescribe the flow rate at the nasopharyngeal face is that the pressure at the outlet is unknown and its flow rate is same as the inlet for steady flow condition.

2.4.4. Computational modelling

An incompressible pressure-based turbulent ($k-\Omega$ SST model) Navier-Stokes flow solver was employed to compute the quasi-steady airflow. An atmospheric air was used as a continuous material across the whole domain. A semi-implicit pressure linked equation scheme, which involves a pressure-velocity coupled solver was implemented to numerically solve the equations simultaneously. Second order upwind discretisation for convective, momentum and pressure were used for higher accuracy with good stability. Solution convergence criteria was that the residuals of the equations to reduce to 10e-4. A mesh convergence study

was conducted to ensure that the computational mesh used was optimal and the results were mesh independent.

Flow on four cross-sectional planes perpendicular to the floor of the nasal cavity (Figure 5) were analysed by examining the streamlines, peak velocity and peak pressure of the airflow in each half of the nose and their longitudinal distribution.

3. Results

3.1. Active anterior rhinomanometry

The volumetric flow rates of inhaled air at the nasal nostrils, were found to be 161/min on the right, 571/min on the left.

3.2. CFD simulation

3.2.1. The streamlines

With the standard data, in the right half of the nose, the entire volume of airflow goes straight along the lower and middle

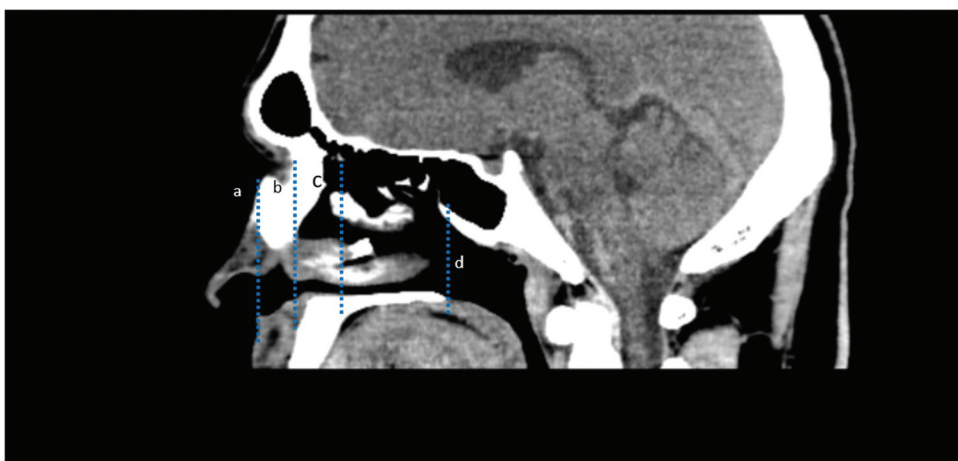


Figure 5. Sagittal view of the nasal cavity (side view) with 4 key planes of the cross section (a) the first area on the nasal vestibule, (b)the second area on the front end of inferior nasal turbinate, (c) the third area on the front end of the middle nasal turbinate/the adjoining part of septum deviation, (d) – the fourth area on the choana (the posterior part of the nasal cavity).

nasal passages, and a small cluster of vortices are noted in the upper part of the nasal cavity, as well as isolated ones under the inferior nasal turbinate and nasopharynx (the soft upper part of the throat, behind the nose) (Figure 6(a)). In the left cavity, the flow streamlines are distributed along the nasal cavity, bypassing the curved part of the septum from above like an arc and below directly, thus repeating the shape of the nasal cavity's top and the lower nasal passage. (Figure 6(b)). There were singular vortexes in the nasal vestibules and even the nasopharynx.

With personal data, the flow direction remains unchanged (Figure 7(b)) in the left half, while on the right side the flow velocity magnitude increases and several arched lines appear in the upper section (Figure 7(a)). The number of vortices was increased in both cavities of the nose, especially in the left nasal vestibule. A similar situation was observed in the upper part on the right side, which coincides with increased air flows in this area.

3.2.2. Peak velocity and peak pressure, their longitudinal distribution

These indicators were estimated for four key cross-sections that were discussed, and a colour scale adjacent to the figures. (Appendices A, B). There were 10 layers in total for this model. With the help of specialist-rhinologist, the appropriate cross-sectional plane for the four required areas was determined (Figure 5) and selected for the study: the 1st section of the nasal vestibulum corresponded to the 2nd layer on the 3D model, the 2nd section of the front end of the inferior nasal turbinate to 5th layer, the 3rd section to 6th layer, and the 4th to 9th layer (Figure 8).

Totally, the peak velocity was higher on the septum deviation side (left) of the nasal cavity. After introducing personal data of mass flow rate for input the peak velocity increased in two nasal halves (Table 1).

For the standard data, in the right cavity, the flow peak velocity decreased gradually (from 8.5 to 2.6 m/s) to the choana. The maximum peak velocity (8.5 m/s) was observed on the vestibulum. With personal data, the peak velocity had the same maximum peak velocity (9.0 m/s) on the nasal valve collapsed. After a short drop to 4.7 m/s, it had a constant decline towards the nasal back (5.2 and 5.0 m/s).

In the left, the peak velocity meaning (6.8–2.4 m/s) also had a gradual decline towards the nasal back. After the introduction of personal input data, the flow rate increased sharply throughout the nasal cavity of 30, 23, and 17.0 m/s in the first three points.

Oppositely, after entering the PD the peak pressure totally decreased in both nasal halves, and the lowest meaning was in the left cavity (-492.5 –18 Pa) with septum deviation (Table 2).

The slow growth of the peak pressure was detected in the right and left sides beside the second section of the left cavity where it increased dramatically from -60.6 Pa to -2.8 Pa. With PD the peak pressure also rose towards the nasal back. The lowest number was at the left nostril (healthy) which also dropped with PD.

4. Discussion

Patient-specific study of the nasal cavity aerodynamics is highly crucial for the diagnostics method of the nasal pathologies

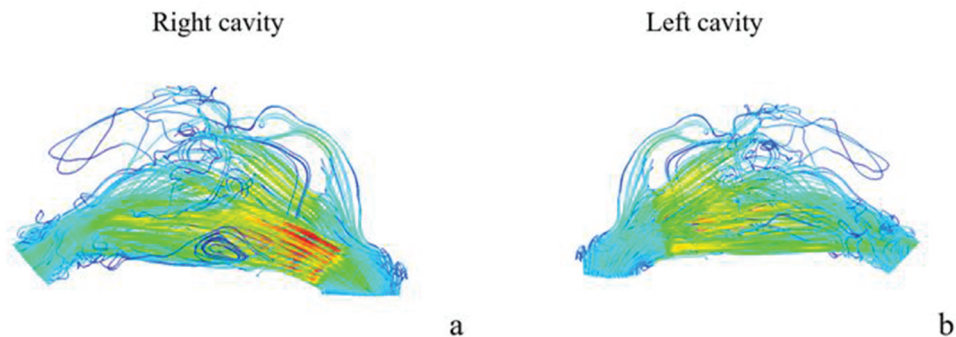


Figure 6. The longitudinal view of the streamlines, velocity magnitudes and vortexes with standard data (SD).

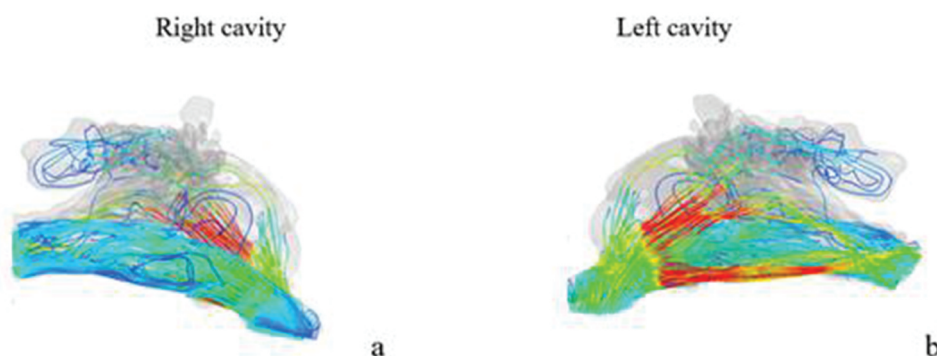


Figure 7. The longitudinal view of the streamlines, velocity magnitudes and vortexes with personal data (PD).

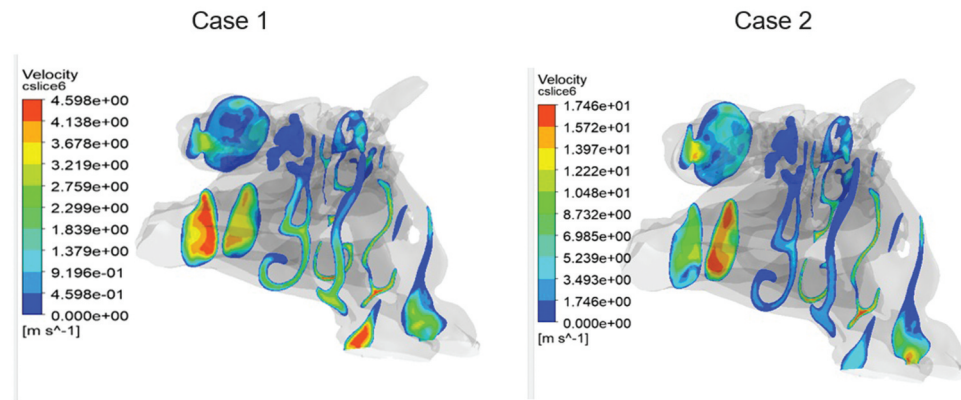


Figure 8. Slices across the longitudinal section is displayed with velocity contours for the standard (a) and personal (b) volume-flowrate through both of the inlets.

Table 1. Right and left peak velocities of four cross-sectional areas with SD and PD, m/s.

The location	SD/Right cavity	SD/Left cavity	PD/Right cavity	PD/Left cavity
First section	8.5	6.8	9.0	30.0
Second section	4.7	6.8	4.7	23.0
Third section	3.6	4.5	5.2	17.0
Fourth section	2.6	2.4	5.0	7.2

Table 2. The peak pressure profiles for the right and left nasal cavities with standard and personal data.

The location	SD/Right cavity	SD/Left cavity	PD/Right cavity	PD/Left cavity
First section	-5.8 Pa	-60.6 Pa	-9.6 Pa	-492.5 Pa
Second section	-5.6 Pa	-2.8 Pa	-9.5 Pa	-235 Pa
Third section	-4.6 Pa	-10.0 Pa	-10.0 Pa	-73 Pa
Fourth section	-1.7 Pa	-1.7 Pa	-5.3 Pa	-18 Pa

based on the computational mechanics of liquids and gases. This topic has been intensively studied and discussed in the literature (Leong et al. 2010; Quadrio et al. 2014). For personalised CFD simulation, patients usually were sub-divided into groups according to the nasal septum deviation types (Li et al. 2019), possible orientations of the nasal valve were modelled (Xi et al. 2016), and by gender and nationality were separated (Zhao et al. 2004; Burgos et al. 2014). Giancarlo B. and others found that some anatomical variations (cross-sectional area and volume) of the nasal cavity and CFD simulation results correlate strongly with applied segmentation thresholds (Cherobin et al. 2018).

In presented patient-specific study, a gap in research related to input data was demonstrated. In our experiment, we employed active anterior rhinomanometry data in the form of volumetric flow rate in 1/min. In the test subject, the flow rates of the left and right nasal cavities were different due to the different anatomical structure of each half. In addition, the flow rate of the left half of the nose (571/min) significantly exceeded the often-used population averaged level (151/min).

The results acquired showed that with standard data the airflow direction on the side of the nasal valve collapse coincides with the results of other studies in the patients with unilateral stenosis of the nasal vestibule (Wang et al. 2016). In a previous

study (Chen et al. 2009), the increase of mass flow rate to 30 l/min only increased the flow velocity magnitudes without changing their directions. We observed similar results in our study: after the introduction of the personal data, the airflow did not change its direction, only the velocity magnitude increased.

de Gabory et al. (2018) used 30 l/min for input in a healthy male, then noted a gradual decrease of the inspiratory flow velocity till the back of the nasal cavity where the velocity again increases. In our case the simulation as with SD as with PD showed the same decline but there was not any growth after.

However, with PD in the right cavity, the velocity had an unsystematic character of decrease towards the nasopharynx (4.7, 5.2, and 5.0 m/s at the second, third and fourth points, respectively). Perhaps this is due to the anteroposterior direction of the septum deviation.

The peak pressure oppositely rose from nostrils to the choanas in both cavities in two cases. No one previous works showed such a result because the peak pressure decreased to the back there. Perhaps, there was no investigation with similar type of nasal pathology or many of them were conducted on healthy patients.

In the previous study conducted by (Li et al. 2019), it was revealed that with a standard flow rate (151/min), in all patients the peak velocity of the nasal cavity on the nasal septum deviation side was higher than the opposite side. The exception was for the 4th type of deviation according to Mladina classification, where the peak velocity was in the middle part of the nasal cavity. As with standard data (SD) as with personal data (PD), we noticed the same phenomenon: in two cases the peak velocity was higher on the deviation side. An increase of input data from 151/min to 571/min on the left side gave a four-fold jump in the flow velocity, which expresses the direct dependence on the input flow rate. A straight proportional growth in a pressure and velocity was also observed in a study where 20 l/min and 34 l/min were used as flow rate (Chen et al. 2009) on the concave side of C-shaped septum deviation. Moreover, in our study with SD the velocity on the left before the deviation is the same for the first 2 zones (6.8 m/s), while with personal data the speed values in these zones are different (30 and 23 m/s). These changes of the velocity meanings on the different sections with PD can more accurately describe the pathological air movement in the S deviation type of nasal septum. Also, all velocity and pressure changes were depended on the input volume, as with 161/min input caused no significant

alterations in the right cavity. So, it was predictable to have a huge drop of pressure and velocity meanings with 571/min input for the left cavity.

The results of reports on nasal airflow simulations showed an increase of air velocity on the anatomical narrow regions (vestibulum, septum deviation halves) (Chen et al. 2009; Wang et al. 2016). We have also observed the maximum peak velocity meanings on the nostrils of both cavities.

These findings indicate that personal data do not change the general tendency of pathological flow in the nasal cavity, but more specifically alter local biophysical parameters.

In general, rhinomanometry can provide volumetric flow rate specific for each patient, which depends on various factors (nasal cavity cross sectional area, direction of the nasal tip, size of the nasopharynx, lower respiratory tract pathology type, weight, nationality) (Serra Battles et al. 1990). However, these factors are very difficult to take into account during CFD simulations of nasal airflow. Therefore, we believe that using the results of active anterior rhinomanometry as input data will bring researchers closer to the personalised diagnosis of each nasal pathology.

Without any doubt, further study with a large number of simulations is required to test the hypothesis.

Rhinomanometric personal data may affect the parameters of CFD simulations, which are compared on virtual and nasal after surgery models. This can significantly improve the quality of the evaluation of the results after virtual surgical manipulation in the nasal cavity.

5. Conclusion

Based on the data of the patient-specific study, we found out that in a patient with unilateral nasal valve collapse and S-shaped septum deviation, personal data do not affect the direction of the streamlines and the peak velocity and pressure distribution, but changes their magnitudes in the different locations of the nasal cavity. A personalised approach will improve the assessment of the results of virtual surgery in the nasal cavity.

6. Limitations and strengths

The main limitation of the study was the participation of only one patient in the experiment. It does not provide a possibility to obtain more information about the influence of personalised data on the simulation results. In order to improve and enhance the study, we have to create several groups according to the nasal septum deviation types from the lighter to the most complex

Disclosure statement

The authors declare that they have no competing interests related to this work.

Funding

This research did not receive any specific grant from funding agencies in the public, commercial, or not-for-profit sectors.

Notes on contributors

Nazym S. Sagandykova, M.D., MMed Department of Otorhinolaryngology Kazakh Medical University of Continuing Education E-mail: doctor.ent.alm@gmail.com Tel: +77018888542; +77775552121. Bachelor: 2001-2007, Semey State Medical Academy with a best student award. Internship: 2007-2008, Otolaryngology, Kazakh Medical University, Astana, Kazakhstan. Residency: 2008-2013, Otolaryngology, Kazakh Medical University of Continuing Education (former Almaty Postgraduate Institute for Physicians) Almaty, Kazakhstan. Master: 2013 – 2015, Medicine, Almaty Postgraduate University for Physicians Almaty, Kazakhstan. Doctoral student of Phd Program: 2018, September, Kazakh Medical University of Continuing Education Almaty, Kazakhstan.

Ildar R. Fakhradiyev, PhD Candidate Experimental Medicine Laboratory, S. D. Asfendiyarov Kazakh National Medical University, E-mail: fakhradiyev.i@kaznmu.kz, Tel: +77075001190. September 2017 to the present Head of Experimental Medicine Laboratory. September 2018 to the present PhD Candidate in S.D. Asfendiyarov Kazakh National Medical University.

Sreekar Reddy Sajjala received Bachelor's in Technology in Mechanical Engineering from BML Munjal University, India, in 2019. He is currently pursuing Master's in Science in Computational Engineering at RWTH Aachen University, Germany. He has worked on a CFD project on a casting process and published a research paper in the Journal of Manufacturing Processes (DOI: <https://doi.org/10.1016/j.jmapro.2019.07.033>). He is also a multi-disciplinary researcher with experience CAD, CAE, ML, Data Analysis and Robotics. His research work includes are Computational Fluid Dynamics, Finite Element Analysis, and Multi-Body Dynamics. E-mail: sreekar2858@gmail.com.

Dr. Saule A. Taukeleva, PhD Professor of Otorhinolaryngology, Kazakh Medical University of Continuing Education E-mail: saule_taukeleva@mail.ru 1970-1977 Almaty Medical Institute, Pediatrics. 1978-1980 1st children's hospital, staff physician. 1980-1986 Almaty City Hospital. 1986-1988 Residency in Otorhinolaryngology, AGIUV, Almaty. 1988-2000 Research assistant in Otorhinolaryngology department, AGIUV, Almaty. 2000-2002 Associate Professor, AGIUV, Almaty. 2002-present Head of Otorhinolaryngology Department, KaMUCE.

Dinara E. Shemetova, MD Department of Otorhinolaryngology (Associate Professor), Kazakh Medical University of Continuing Education, e-mail: toguzbayeva@list.ru. June 2005 - November 2009 otorhinolaryngologist at the City Clinical Hospital No. 5 in Almaty. November 2009 - September 2012 otorhinolaryngologist at the City Polyclinic in Kokshetau. September 2012 to May 2014 - Assistant at the Department of Otorhinolaryngology, AGIUV. May 2014 to the present, Associate Professor of the Department of Otorhinolaryngology KazMUCE. February 2017 to the present - General Director and Doctor of the ENT Center V-ent.

Timur M. Saliev, PhD Scientific Research Institute of Fundamental and Applied Medicine named after B. Atchabarov, S.D. Asfendiyarov Kazakh National Medical University, E-mail: tim.saliev@gmail.com, Tel: +77024150420. September 2018 to the present Director of Scientific Research Institute of Fundamental and Applied Medicine named after B. Atchabarov.

Shynar B. Tanabayeva, PhD Candidate Experimental Medicine Laboratory, S.D. Asfendiyarov Kazakh National Medical University, E-mail: shynar.tanabayeva@mail.ru, Tel: +77772569060. September 2019 to the present PhD Candidate in S.D. Asfendiyarov Kazakh National Medical University.

Dr. Yong Zhao, PhD Department of Mechanical Aerospace Engineering, School of Engineering, Nazarbayev University Email: yong.zhao@nu.edu.kz Tel : +(966-1) 215-7755 office Education: Ph.D. 1992 University of Manchester, UK. Mechanical Engineering MSc. 1989 University of Manchester, UK. Mechanical Engineering B.Sc. 1985 Xi'an Jiaotong University, PR China with best student award. Power Machinery Engineering Summary Professional Experience: Jan 1991 - Mar 1992 Research Associate, the University of Manchester 29 Mar 1992 - 28 Mar 1995 Research Fellow, Nanyang Technological University (NTU), Singapore 29 Mar 1995 - 31 Dec 1998 Lecturer, NTU 1 Jan 1999 - 31 Dec 2000 Assistant Professor, NTU 1 Jan 2001 – 31 December 2009 Associate Professor, NTU (10-year (2003) and 15-year Long Service Awards from NTU (2008)) 06

February 2010-30 August 2016, Chair of mechanical engineering and Chair of advisory board, Chair (VD) of Research of College of Engineering and member of college management board, Alfaisal University, Riyadh, Kingdom of Saudi Arabia (interviewed at MIT and selected by a group of senior Professors from MIT and Cambridge University) Jan 2015-present, Haitian Professor, Dalian University of Technology, Dalian, PRC September 2016-Present, Professor of Mechanical and Aerospace Engineering, School of Engineering, Nazarbayev University, Republic of Kazakhstan.

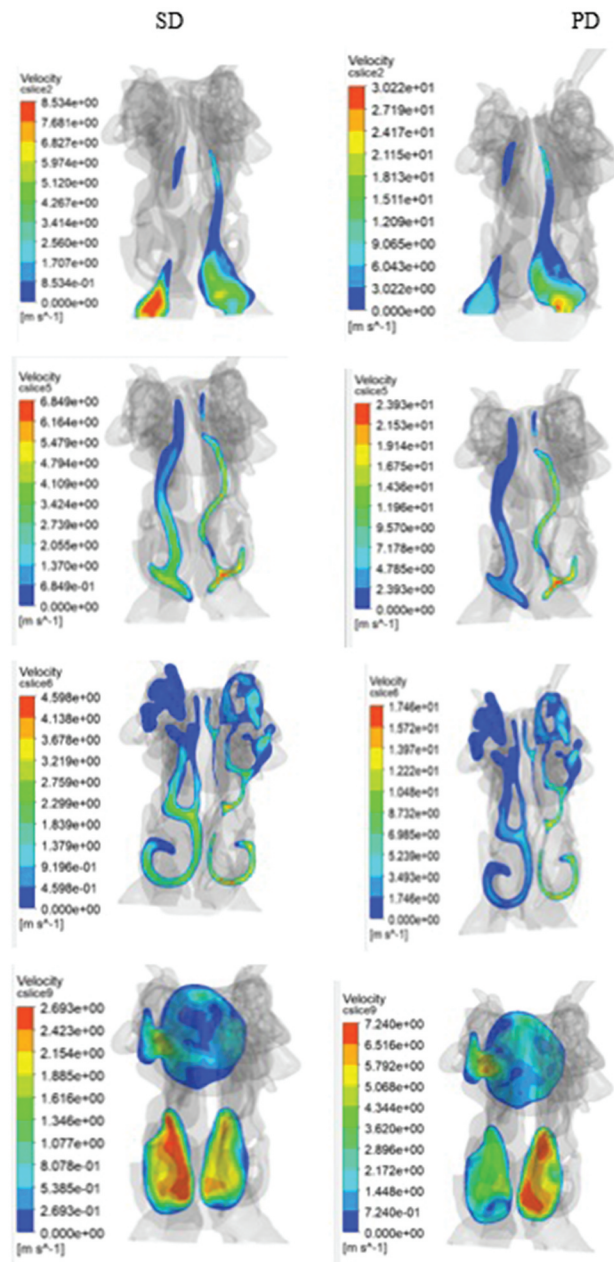
ORCID

Nazym S. Sagandykova  <http://orcid.org/0000-0002-7274-8101>
Yong Zhao  <http://orcid.org/0000-0002-9574-4787>

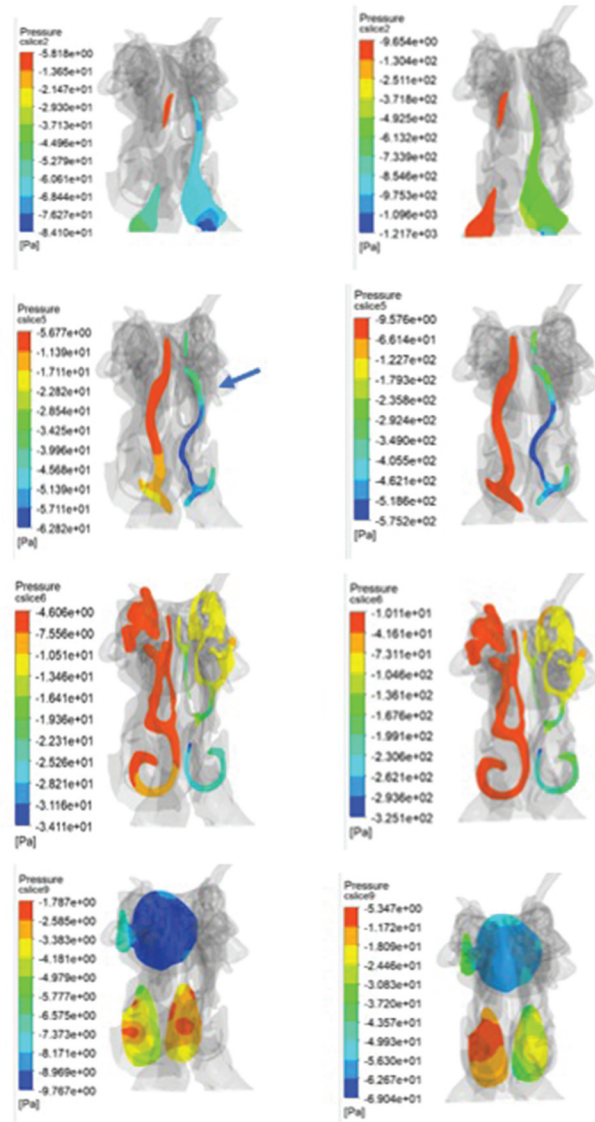
References

- Bavo AM, Pouch AM, Degroote J, Vierendeels J, Gorman JH, Gorman RC, Segers P. 2016. Patient-specific CFD simulation of intraventricular haemodynamics based on 3D ultrasound imaging. *Biomed Eng Online*. 15(1):107. eng. doi:[10.1186/s12938-016-0231-9](https://doi.org/10.1186/s12938-016-0231-9).
- Burgos MA, Sanmiguel-Rojas E, Martín-Alcántara A, Hidalgo-Martínez M. 2014. Effects of the ambient temperature on the airflow across a Caucasian nasal cavity. *Int J Numer Method Biomed Eng*. 30(3):430–445. eng. doi:[10.1002/cnm.2616](https://doi.org/10.1002/cnm.2616).
- Chen XB, Lee HP, Chong VF, Wang de Y. 2009. Assessment of septal deviation effects on nasal air flow: a computational fluid dynamics model. *The Laryngoscope*. 119(9):1730–1736. eng. doi:[10.1002/lary.20585](https://doi.org/10.1002/lary.20585).
- Cherobin GB, Voegels RL, Gebrim E, Garcia GJM, Tang D. 2018. Sensitivity of nasal airflow variables computed via computational fluid dynamics to the computed tomography segmentation threshold. *PLoS One*. 13(11):e0207178. eng. doi:[10.1371/journal.pone.0207178](https://doi.org/10.1371/journal.pone.0207178).
- Cho S-I, Hauser R, Christiani DC. 1997. Reproducibility of nasal peak inspiratory flow among healthy adults: assessment of epidemiologic utility. *Chest*. 112(6):1547–1553. eng. doi:[10.1378/chest.112.6.1547](https://doi.org/10.1378/chest.112.6.1547).
- Clement PA, Gordts F. 2005. Consensus report on acoustic rhinometry and rhinomanometry. *Rhinology*. 43(3):169–179. eng.
- de Gabory L, Reville N, Baux Y, Boisson N, Bordenave L. 2018. Numerical simulation of two consecutive nasal respiratory cycles: toward a better understanding of nasal physiology. *Int Forum Allergy Rhinol*. 8(6):676–685. eng.
- Desvant C, Guislain J, Vandenhende-Szymanski C, Mortuaire G. 2018. The correlation between active anterior rhinomanometry results and nasal obstruction symptoms scores after inferior turbinate reduction: A prospective cohort study about sixty-five patients. *Clin Otolaryngol*. 43(4):1153–1156. eng.
- Doorly D, Taylor DJ, Franke P, Schroter RC. 2008a. Experimental investigation of nasal airflow. *Proc Inst Mech Eng H*. 222(4):439–453. eng.
- Doorly DJ, Taylor DJ, Schroter RC. 2008b. Mechanics of airflow in the human nasal airways. *Respir Physiol Neurobiol*. 163(1–3):100–110. eng.
- Elad D, Wolf M, Keck T. 2008. Air-conditioning in the human nasal cavity. *Respir Physiol Neurobiol*. 163(1–3):121–127. eng.
- Enberg RN, Ownby DR. 1991. Peak nasal inspiratory flow and Wright peak flow: a comparison of their reproducibility. *Ann Allergy*. 67(3):371–374. eng.
- Hirschberg A, Rezek O. 1998. Correlation between objective and subjective assessments of nasal patency. *ORL J Otorhinolaryngol Relat Spec*. 60(4):206–211. eng.
- Hooper RG. 2001. Forced inspiratory nasal flow-volume curves: a simple test of nasal airflow. *Mayo Clin Proc*. 76(10):990–994. eng.
- Hsu HC, Tan CD, Chang CW, Chu CW, Chiu YC, Pan CJ, Huang HM. 2017. Evaluation of nasal patency by visual analogue scale/nasal obstruction symptom evaluation questionnaires and anterior active rhinomanometry after septoplasty: a retrospective one-year follow-up cohort study. *Clin Otolaryngol*. 42(1):53–59. eng.
- Huygen PL, Klaassen AB, de Leeuw TJ, Wentges RT. 1992. Rhinomanometric detection rate of rhinoscopically-assessed septal deviations. *Rhinology*. 30(3):177–181. eng.
- Leong SC, Chen XB, Lee HP, Wang DY. 2010. A review of the implications of computational fluid dynamic studies on nasal airflow and physiology. *Rhinology*. 48(2):139–145. eng.
- Li L, Zang H, Han D, London NR Jr. 2019. Impact of varying types of nasal septal deviation on nasal airflow pattern and warming function: a computational fluid dynamics analysis. *Ear Nose Throat J*. 145561319872745. eng.
- Liu T, Han D, Wang J, Tan J, Zang H, Wang T, Li Y, Cui S. 2012. Effects of septal deviation on the airflow characteristics: using computational fluid dynamics models. *Acta Otolaryngol*. 132(3):290–298. eng.
- Quadrio M, Pipolo C, Corti S, Lenzi R, Messina F, Pesci C, Felisati G. 2014. Review of computational fluid dynamics in the assessment of nasal air flow and analysis of its limitations. *Eur Arch Otorhinolaryngol*. 271(9):2349–2354. eng.
- Riazuddin VN, Zubair M, Abdullah MZ, Ismail R, Shuaib IL, Hamid SA, Ahmad KA. 2011. Numerical study of inspiratory and expiratory flow in a human nasal cavity. *J Med Biol Eng*. 31(3):201–206. doi:[10.5405/jmbe.781](https://doi.org/10.5405/jmbe.781).
- Serra Batllés J, Montserrat JM, Martos JA, Picado C, Agustí Vidal A. 1990. Anterior rhinomanometry. An Otorrinolaringol Ibero Am. 17(2):159–164. spa.
- Sipilä J, Suonpää J, Silvoniemi P, Laippala P. 1995. Correlations between subjective sensation of nasal patency and rhinomanometry in both unilateral and total nasal assessment. *ORL J Otorhinolaryngol Relat Spec*. 57(5):260–263. eng.
- Taylor DJ, Doorly DJ, Schroter RC. 2010. Inflow boundary profile prescription for numerical simulation of nasal airflow. *J R Soc Interface*. 7(44):515–527. eng.
- Wang T, Chen D, Wang PH, Chen J, Deng J. 2016. Investigation on the nasal airflow characteristics of anterior nasal cavity stenosis. *Braz J Med Biol Res*. 49(9):e5182. eng.
- Wen J, Inthavong K, Tu J, Wang S. 2008. Numerical simulations for detailed airflow dynamics in a human nasal cavity. *Respir Physiol Neurobiol*. 161(2):125–135. eng.
- Xi J, Kim J, Si XA. 2016. Effects of nostril orientation on airflow dynamics, heat exchange, and particle depositions in human noses. *Eur J Mech - B/ Fluids*. 55:215–228.
- Xiong GX, Zhan JM, Jiang HY, Li JF, Rong LW, Xu G. 2008. Computational fluid dynamics simulation of airflow in the normal nasal cavity and paranasal sinuses. *Am J Rhinol*. 22(5):477–482. eng.
- Zhao K, Scherer PW, Hajiloo SA, Dalton P. 2004. Effect of anatomy on human nasal air flow and odorant transport patterns: implications for olfaction. *Chem Senses*. 29(5):365–379. eng.

Appendices



Appendix A. The peak velocity profiles in 4 cross sectional planes in two cases: (a) vestibulum, (b) the anterior end of inferior turbinate, (c) the head of middle turbinate, (d) the posterior part of inferior turbinate/choana. The coloured velocity scale is attached.



Appendix B. The peak pressure profiles in 4 cross sectional planes in two cases: (a) vestibulum, (b) the anterior end of inferior turbinate, (c) the head of middle turbinate, (d) the choana. The coloured pressure scale is attached.